Chem Biol Drug Des 2012; **79:** 9–21
© 2011 John Wiley & Sons A/S
doi: 10.1111/j.1747-0285.2011.01249.x

Research Article

Exploring the Interaction Between siRNA and the SMoC Biomolecule Transporters: Implications for Small Molecule–Mediated Delivery of siRNA

Matt Gooding[1], Slavica Tudzarova[1], Roberta J. Worthington[2], Sarah R. Kingsbury[1], Anne-Sophie Rebstock[1], Henry Dube[1], Michela I. Simone[3], Cristina Visintin[1], Dimitris Lagos[4,†], Juan-Manuel Funes Quesada[4], Heike Laman[5], Chris Boshoff[4], Gareth H. Williams[1], Kai Stoeber[1] and David L. Selwood[1,*]

[1]*The Wolfson Institute for Biomedical Research, UCL, Gower Street, London WC1E 6BT, UK*
[2]*Department of Chemistry, North Carolina State University, Raleigh, NC 27695, USA*
[3]*School of Chemistry, University of Sydney, Sydney, NSW 2006, Australia*
[4]*UCL Cancer Institute, UCL, London WC1E 6BT, UK*
[5]*Division of Cellular and Genetic Pathology, Department of Pathology, University of Cambridge, Tennis Court Road, Cambridge CB2 1QP, UK*
**Corresponding author: David L. Selwood, d.selwood@ucl.ac.uk*
[†]*Present address: Centre for Immunology and Infection, Department of Biology and Hull York Medical School University of York, York YO10 5DD, UK.*

The small molecule carrier class of biomolecule transporters, modeled on the third helix of the Antennapedia homeodomain, has previously been shown to transport active proteins into cells. Here, we show an improved synthetic route to small molecule carriers, including Molander chemistry using trifluoroborate salts to improve the yield of the Suzuki–Miyaura coupling step for the formation of the biphenyl backbone. The required boronic acids could be formed by the reaction of a 2-(dimethylamino)ethyl ether-modified aryl Grignard reagent with triisopropyl borate. The potential for the use of small molecule carriers as oligonucleotide-transporting agents was also explored by characterizing the interactions between small molecule carriers and siRNA. Molecular dynamics and NMR analysis indicated that the small molecule carrier guanidines are stabilized by π-cation interactions with the biphenyl system, thus not only increasing the basicity or pKa but also shielding the charge. The binding affinities of various small molecule carriers for siRNA were investigated using isothermal calorimetry and gel shift assays. Small molecule carrier-mediated siRNA delivery to cultured fibroblasts is demonstrated, showing that small molecule carriers possess the ability to transport functional siRNA into cells. Knockdown of Cdc7 kinase, a target for cancer, is achieved.

Key words: calorimetric techniques, chemical biology, molecular modeling, nanotechnology (drug discovery), RNAi and antisense techniques

Received 14 July 2011, revised 12 September 2011 and accepted for publication 24 September 2011

The use of short interfering RNA (siRNA) to knockdown target genes via the mechanism of RNA interference (RNAi) has received much attention over the last decade owing to the wide-ranging therapeutic implications of this technology. Indeed, the first clinical trials of siRNA-based drugs have started to emerge in recent years, with many more potential targets having been identified both *in vitro* and *in vivo* (1,2). There are, however, major challenges to the development of RNAi therapeutics, including degradation, specificity, and delivery. To knockdown its target gene, the siRNA must enter the cell and bind to a protein complex called the RNA-induced silencing complex (RISC) (3). siRNA molecules are large and highly negatively charged, rendering them unable to cross the lipid bilayer of the cell membrane. Therefore, the development of a safe, effective delivery agent for siRNA remains one of the biggest challenges in biological therapeutics.

Several types of delivery vectors have been successfully used to transport RNA into cells, including liposomes (4), cationic polymers (5), and cell-penetrating peptides (CPPs) (6–9). Among the CPPs that have been shown to be successful in delivering siRNA are TAT, penetratin, transportan, and polyarginine (8). Amphipathic CPPs, which display both cationic and lipophilic residues in the same molecule, have been shown to be particularly effective delivery agents, and several successful synthetic amphipathic CPPs have been designed, such as CADY (7,10) and MPG (9). Although the mechanism for CPP transduction is yet to be fully revealed, it is thought that crucial steps include binding to negatively charged cell-surface proteoglycans (7,11,12), followed by endocytotic internalization, translocation (12), and endosomal escape (13). The mechanism for internalization (14) has been widely debated, and recent studies point to multiple mechanisms operating (12, 15) with peptide structure playing a key role.

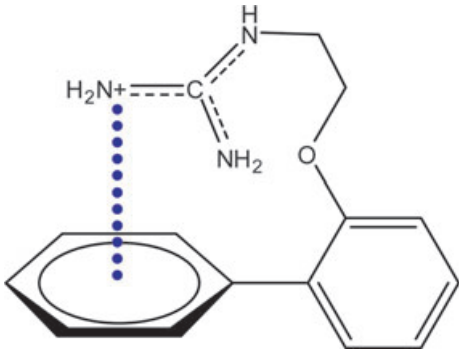

Figure 1: Illustration of the π-cation effect for a biphenyl small molecule carrier molecule.

π-Cation interactions were first described by Burley and Petsko in 1986 (16) when they observed that the side chains of cationic amino acids such as lysine and arginine are preferentially located near the π-electron cloud of aromatic amino acids such as phenylalanine, tyrosine, and tryptophan. It has been found that π-cation interactions are very common in proteins, with one interaction per 77 residues on average. Arginine residues are more favored for π-cation interactions than lysine, probably due to the guanidine group on arginine being larger and less solvated, resulting in greater van der Waals interactions with aromatic rings than that of lysine, as well as the ability of guanidines to form hydrogen bonds and π-cation interactions simultaneously, whereas the lysine side chain can only participate in one type of binding at a time (17).

Previously, we reported on a class of small molecule carriers (SMoCs) based on amphipathic CPPs that were capable of delivering functional proteins into cells (Figure 1) (18). We hypothesize that as SMoCs mimic guanidine-rich CPPs, possessing guanidinium cations linked to a lipophilic biphenyl system (19), they may be able to internalize siRNA in the same way as amphipathic CPPs such as MPG. The positively charged guanidinium cations also enable the formation of electrostatic complexes with siRNA as have been observed for several cationic peptides (6,10,20). In this paper, we study the potential for SMoCs to form non-covalent complexes with siRNA by investigating the pKa of the SMoC guanidine groups, as well as measuring the affinity of different SMoCs for siRNA. We also examine the intramolecular structure of the SMoCs and provide evidence to indicate that the guanidine groups are stabilized by π-cation interactions (Figure 1) (17). Moreover, we explore whether these simple SMoCs may be used as siRNA delivery agents *in vitro*.

Materials and Methods

Synthetic chemistry

Starting materials were either commercially available or synthesized according to methods reported in the literature. ^{1}H and ^{13}C NMR spectra were recorded on a Bruker AMX-300 or a Bruker AMX-500 spectrometer (Bruker BioSpin GmbH, Rheinstetten, Germany). Chemical shifts are reported as p.p.m. relative to TMS internal standard. Mass spectra were recorded on a Fisons VG70-SE spectrometer (EI, FAB) or an Agilent 6100 Series LC-mass spectrometer using a C-18 or C-4 column. Microwave reactions were carried out using a CEM Discover microwave (CEM Corporation, Matthews, NC, USA). Polyarginine peptides were obtained from Peptide Protein Research, Hampshire, UK. siRNA sequences were purchased from Dharmacon RNAi Technologies (Thermo Fisher Scientific, Dharmacon Products, Lafayette, CO, USA). The sequences used were glyceraldehyde-3-phosphate dehydrogenase (GAPDH) sense 5′ UGG UUU ACA UGU UCC AAU AUU 3′ and antisense 5′ Phosphate U AUU GGA ACA UGU AAA ACC UU 3′; *CDC7* sense 5′ GCU CAG CAG GAA AGG UGU UUU 3′ and antisense 5′ AAC ACC UUU CCU GCU GAG CUU.

Molecular dynamics

Molecular dynamics simulations were run for compounds **14**, **18**, **19**, and **20** in the YASARA (21) software and using the AMBER99 force field with default parameters. The starting structures were contained in a simulation cell which extended 5 Å larger than the SMoC structure along each axis *in vacuo*, the default pH was set to 7.0, and the structures were minimized under the AMBER99 force field (22) starting at 298 K for 1 pseconds. The simulation substep time was set to 1 fseconds, and the intramolecular forces were recalculated every two substeps and the temperature was controlled by velocity rescaling. A 5-nseconds simulation was performed for each structure, after which snapshots were taken and analyzed in the DS VISUALIZER software (Accelrys Inc, San Diego, CA, USA). No atoms were kept frozen during the simulations.

NMR study

The SMoC compounds were dissolved in 0.5 mL deuterium oxide to a final concentration of around 10 mg/mL; 100 mM NaOH was added in small aliquots (5-30 μL) and the pH of the solution measured in the NMR tube using a microelectrode attached to a pH meter. NMR spectra were recorded using a 400-MHz Bruker spectrometer at 20 °C.

Gel shifts

A concentration of 1.7 nmol GAPDH siRNA (Dharmacon RNAi Technologies) was mixed in RNAse-free water with varying concentrations of either SMoC, tetra-arginine, or octa-arginine in the molar ratios of 1/1, 1/5, 1/10, 1/20, and 1/50. The complexes were incubated for 30 min at room temperature. The samples were diluted with loading buffer containing 95% formaldehyde, 0.025% SDS, 0.025% bromophenol blue, 0.025% xylene cyanol FF, 0.025% ethidium bromide, and 0.5 mM EDTA (Thermo Fisher Scientific, Fermentas Products, Lafayette, CO, USA) and analyzed by gel electrophoresis on a 1% agarose gel in a running buffer containing 6.7% formaldehyde, 0.04 M 3-morpholinopropane-1-sulfonic acid,

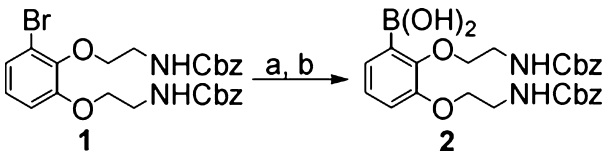

Figure 2: Boronic acid synthesis. Reagents: (a) bis[2-(*N*,*N*-dimethylamino)ethyl] ether, ^{i}PrMgCl, THF, 10–15 °C, 24 h; (b) trimethyl borate, THF, room temperature, 1 h (40%).

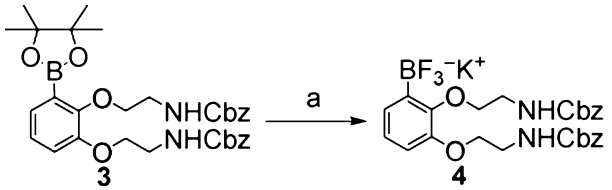

Figure 3: Conversion of boronic ester to trifluoroborate salt. Reagents: (a) aqueous potassium bifluoride, MeOH, room temperature, 3 h (88%).

0.01 M sodium acetate, and 0.001 M EDTA. The gels were analyzed by UV illumination, and the ethidium bromide-stained bands were quantified using the IMAGEJ software (http://rsb.info.nih.gov/ij/). The EtBr intensities were plotted, a dose–response curve was fitted, and EC_{50} values were calculated using the ORIGIN software.

Isothermal calorimetry (ITC)

6G-SMoC at a concentration of 250 μM was loaded into the syringe of a Microcal VP-ITC calorimeter (450 μL), and the cell (1.8 mL)

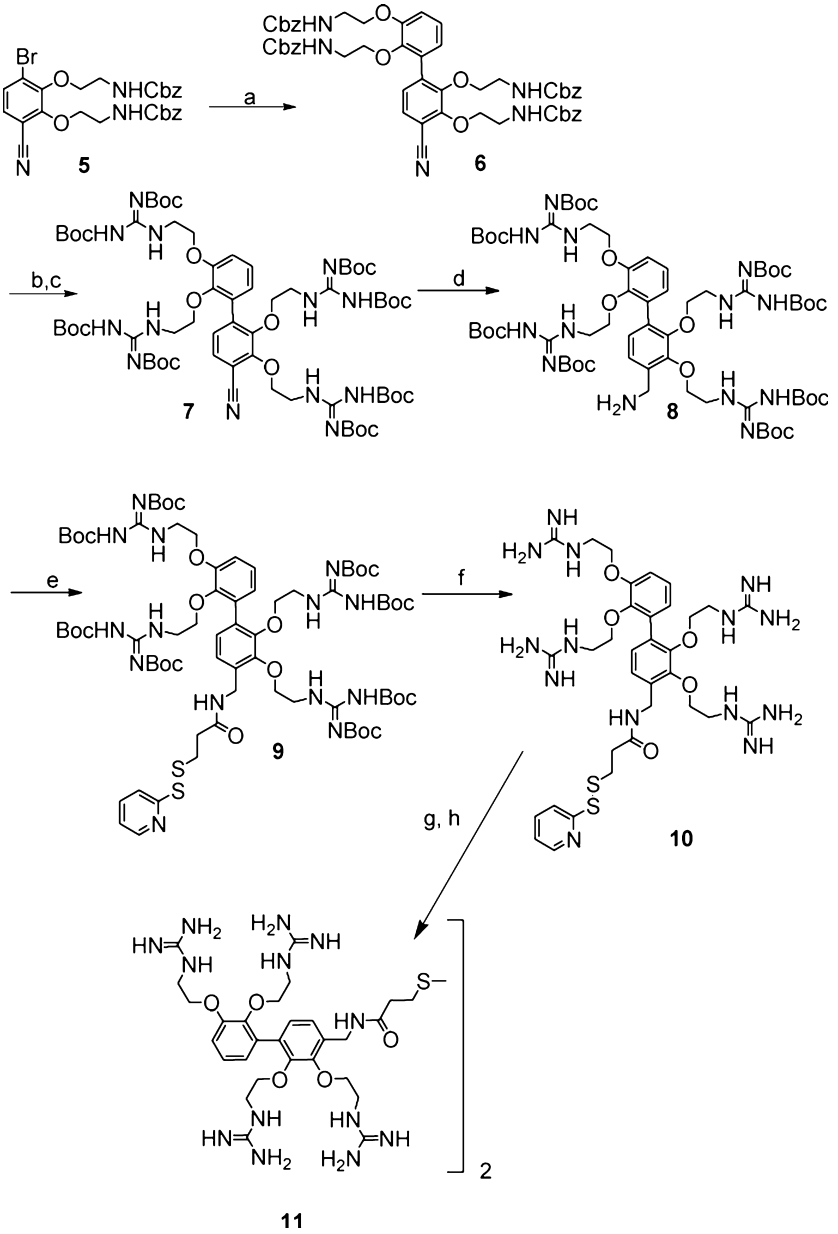

Figure 4: New synthetic route to 4G-small molecule carrier. Reagents: (a) **4**, $PdCl_2dppf{\cdot}CH_2Cl_2$, Et_3N, iPrOH/H_2O, 82 °C, 18 h (79%); (b) 30% HBr in acetic acid, DCM, room temperature, 1 h; (c) *N,N'*-Di-Boc-1H-pyrazole-1-carboxamidine, DIEA, DCM, room temperature, 18 h (71% over two steps); (d) $CoCl_2{\cdot}6H_2O$, $NaBH_4$, MeOH, room temperature, 1 h (60%); (e) 2,5-dioxopyrrolidine-1-yl-3-(pyridine-2-yldisulfanyl)propanoate, DIEA, DCM, room temperature, 18 h (57%); (f) TFA/m-cresol, DCM, room temperature, 3 h (82%); (g) dithiothreitol, H_2O; (h) ammonium acetate, air.

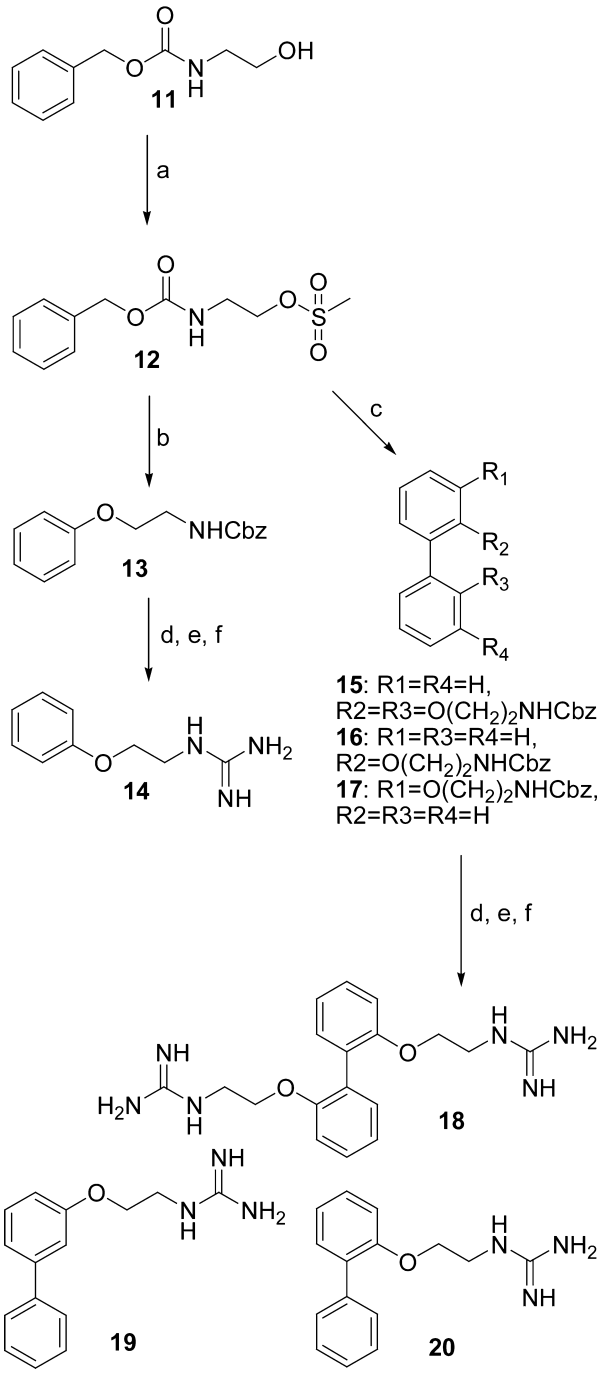

Figure 5: Synthesis of simple small molecule carrier compounds for the determination of guanidine pKa. Reagents: (a) phenol, Cs_2CO_3, acetone, 17 h, 65 °C (70%); (b) 2-,3-, or 2,2′- hydroxybiphenol, Cs_2CO_3, acetone, 17 h, 65 °C (**15**: 35%; **16**: 93%; **17**: 100%); (c) 30% HBr in acetic acid, DCM, 3 h, room temperature; (d) *N,N*′-Di-Boc-1H-pyrazole-1-carboxamidine, DIPEA, MeCN, 48 h, room temperature (**13a**: 45%; **15a**: 51%; **16a**: 26%; **17a**: 40%); (e) TFA/TIPS/H_2O, 4 h, room temperature (100%).

was filled with human GAPDH siRNA (Dharmacon RNAi Technologies) at a concentration of 3.5 μM. A total of 37 injections of 8 μL each were made at 4-min intervals to ensure total saturation of the siRNA. The binding curve was plotted using ORIGIN 6.0 (Microcal) and the binding constants were calculated.

Cell culture and cell cycle analysis

IMR90 (ATCC# CCL-186), a diploid primary human fibroblast adherent cell line derived from fetal lung tissue, was obtained from LGC Standards (Middlesex, UK) at population doubling (PD) 12. All culture passages and population doublings were recorded, and experiments were performed with IMR90 cells under a PD of 22. IMR90 cells were cultured at 37 °C with 5% CO_2 in DMEM (Invitrogen, Paisley, UK) supplemented with 10% defined FCS (Invitrogen), 100 U/mL penicillin, and 100 μg/mL streptomycin.

Immunoblotting

For Western blot analysis, cells were harvested and whole-cell extract (WCE) was prepared in modified RIPA lysis buffer (50 mM Tris–HCl, 300 mM NaCl, 1% NP40, 0.5% sodium deoxycholate, 0.1% SDS, 1 mM EDTA, and protease inhibitors). After sonication of lysates for 10 seconds, protein concentration was determined using the DC Bio-Rad protein assay kit (Bio-Rad, Hemel Hempstead, UK). Forty micrograms of total protein was loaded in each lane and separated by 4–20% SDS-PAGE. Protein was transferred from polyacrylamide gels onto PVDF membranes (Bio-Rad) by semi-dry electroblotting. Blocking, antibody incubations, and washing steps were performed as described (23). Antibodies used for immunoblotting included $p21^{WAF1}$ from BD Biosciences (Oxford, UK), p53 (Ab-6) from Merck (Beeston, UK), Cdc7 from MBL International (Woburn, MA, USA), β-actin from Sigma (Gillingham, UK), and Mcm2 phospho-Ser-40/41 from Bethyl Laboratories (Montgomery, TX, USA). Affinity-purified rabbit polyclonal antibodies for activator of S-phase kinase (ASK - a cell cycle kinase which binds cdc7) were generated by Eurogentec (Seraing, Belgium) following the manufacturer's protocol.

Immunofluorescence

The transfection efficiency of SMoC compared with Lipofectamine 2000 was determined with fluorescein-conjugated non-specific siRNA-transfected cells (FO) (BLOCK-iT Transfection Optimization kit; Invitrogen) using a Leica TCS SP confocal fluorescence microscope. IMR-90 fibroblasts grown on coverslips were treated for 24 h with complexes of 4G SMoC (40 μg/mL, 35 μM) and either 10 nM FO, 100 nM FO, or 100 nM FO without SMoC. After the treatment, cells were washed in PBS and fixed in 3.7% paraformaldehyde. Following fixation, cells were treated with 0.1% Triton X in PBS, blocked with 1% BSA in PBS for 1 h and mounted directly, or first stained with AlexaFluor 546 Phalloidin according to the manufacturer's instructions (Invitrogen) and then mounted in Vectashield mounting medium (Vector Laboratories, Peterborough, UK) with 1.5 μg/mL 4′,6-diamidino-2-phenylindole (DAPI) to visualize DNA.

RNA interference

CDC7 expression was inhibited with double-stranded RNA oligo for CDC7 synthesized by Ambion (Warrington, UK) in complex with Lipofectamine 2000 (Invitrogen) as described previously (24) or with 4G SMoC. Briefly, IMR90 cells were seeded at a density to reach

50% confluence on the day of transfection. The transient transfections were performed using 10 nM of CDC7 siRNA duplex for 72 h. siRNAs were complexed with transfection reagent in serum-free and antibiotic-free culture medium. Selective silencing of the corresponding gene was confirmed by qRT-PCR and Western blotting.

RNA extraction and qRT-PCR

To evaluate the efficiency of transfection with CDC7 siRNA using SMoC compared with Lipofectamine 2000, CDC7 mRNA levels were determined by qRT-PCR as described earlier (24). Briefly, total RNA was isolated using a PureLink Micro-to-Midi kit (Invitrogen) according to the manufacturer's instructions. Reverse transcription reactions using 40 ng of total RNA in a final reaction volume of 20 μL were performed in one step using SuperScript III Platinum SYBR Green One Step qRT-PCR Kit (Invitrogen). Relative quantitative data were obtained using the comparative C_t method with Realplex software according to the manufacturer's protocol (Eppendorf, Heidelberg, Germany). Glyceraldehyde-3-phosphate dehydrogenase was used to normalize each of the extracts for amplifiable human DNA. Primers were provided by Eurofins MWG Operon (Ebersberg, Germany). Cycle conditions are available upon request.

Results and Discussion

Improved SMoC synthetic route to 4G-SMoC

Previously, we described the synthesis of a phenyl boronic ester that acts as a key intermediate in the SMoC synthetic pathway (18). The boronic ester takes part in a Suzuki–Miyaura coupling which generates the biphenyl backbone of the SMoC structure, linked via ether bonds to Z-protected amine groups. As an alternative to the boronic ester, we investigated the formation of the equivalent boronic acid from the aryl bromide **1** using a Grignard reagent with 2-(dimethylamino)ethyl ether followed by quenching with trimethyl borate to yield the boronic acid **2** (Figure 2). As described by Wang *et al.* (25), the organic ligand moderates the reactivity of the aryl Grignard reagent in this reaction, reducing possible side reactions. Careful control of the reaction temperature was required to obtain a synthetically useful yield of 40%.

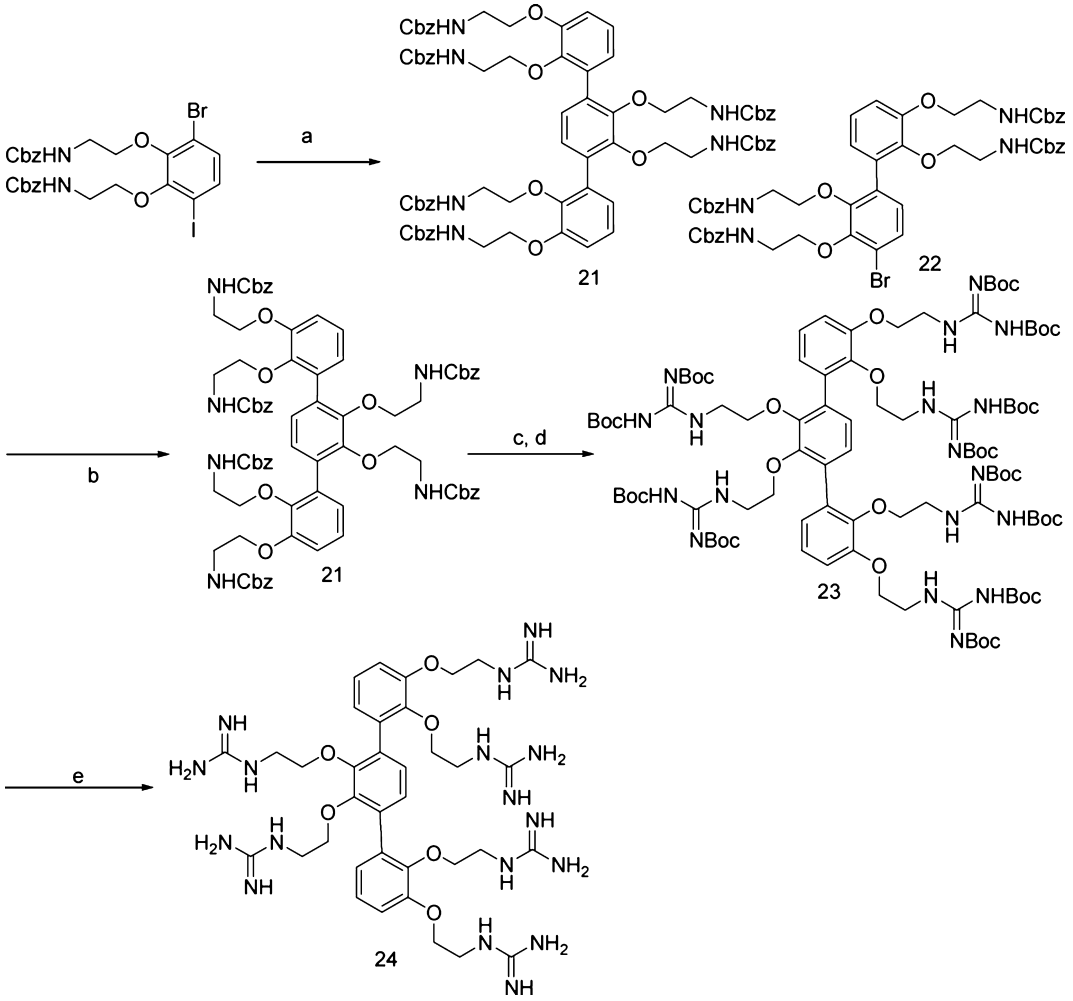

Figure 6: 6G-small molecule carrier synthesis. Reagents: (a) $PdCl_2$dppf, K_3PO_4, toluene, water, 100 °C 3 h; (b) $PdCl_2$dppf, K_3PO_4, toluene, water, 100 °C overnight (48% over two steps); (c) 30% HBr in acetic acid, DCM, room temperature; (d) *N*, *N*-di-boc-*N'*-trifluoromethanesulfonyl-guanidine, DIPEA, DCM, room temperature, overnight (54% over two steps); (e) TFA/TIPS/H_2O, 4 h, room temperature (100%).

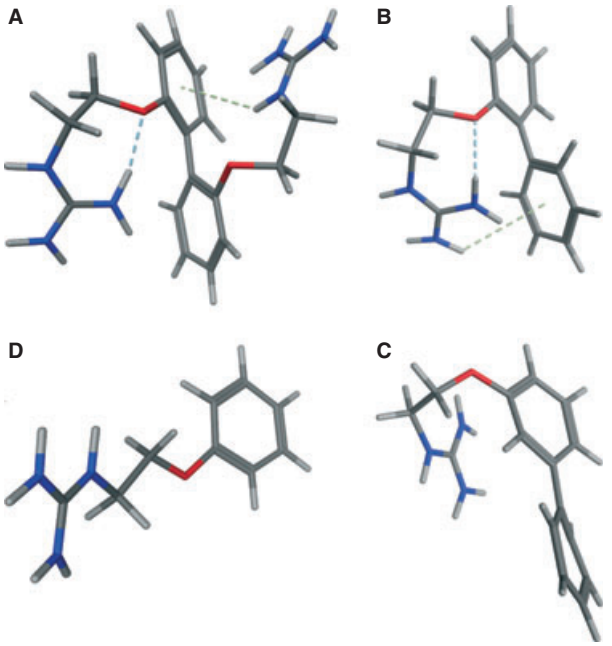

Figure 7: Snapshots of a molecular dynamics simulation of simple small molecule carrier (SMoC)-like molecules containing one or two guanidine side chains. In a simple 2G-SMoC molecule (A), T-shaped π-cation interactions form between the side chains and their opposite rings. This is also the case when one side chain is removed (B). For a monophenyl structure with one side chain (C), no interaction is present, whereas the addition of a second ring *meta* to the side chain (D) promotes a parallel π-cation interaction onto the adjacent ring.

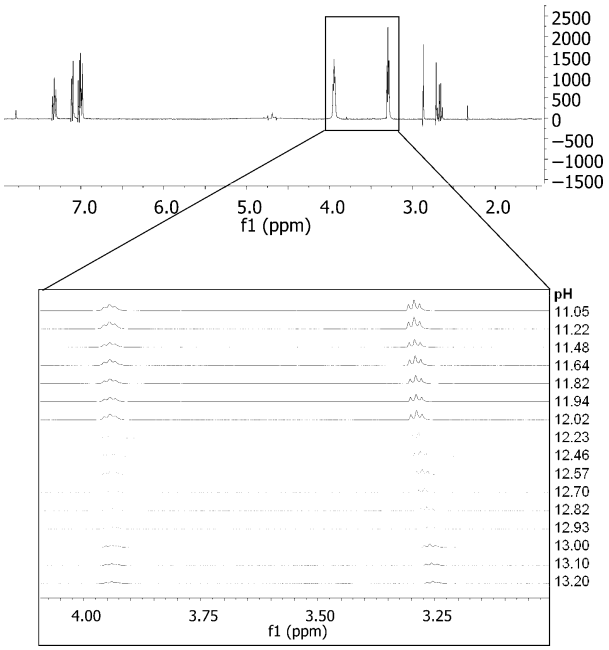

Figure 8: Change in small molecule carrier NMR spectrum as the pH of the solution is increased. Expanded section of NMR spectrum of 18 showing the two triplets corresponding to the four ethyl protons at varying pH values. The CH_2 adjacent to the guanidine group (peak at ~3.3 p.p.m.) becomes less shielded at higher pH values, resulting in a shift in the NMR peak, whereas the other peak (3.97) remains static.

In addition, the potassium trifluoroborate salt was synthesized (Figure 3). Trifluoroborate salts, developed by Molander *et al.* (26,27), are extremely stable to air and moisture, allowing large-scale synthesis of this key intermediate for long-term storage. The pinacolboronate ester **3** synthesized previously was treated with potassium bifluoride in methanol, resulting in an 88% yield of the salt **4**, which is precipitated from the reaction mixture and is easily isolated by filtration and washing with organic solvents. Suzuki reactions with this salt and the alkylated nitrile **5** gave cleaner conversion to the biphenyl **6** with less of the deboronated side product that was difficult to separate from the desired product.

A problematic step in the original SMoC synthesis was the addition of Boc-protected guanidine groups using the expensive *N,N*-di-Boc-*N′*-trifluoromethanesulfonyl-guanidine reagent, which resulted in modest yields. To improve this step, a less expensive and more stable guanidinylation reagent was used, *N,N′*-Di-Boc-1*H*-pyrazole-1-carboxamidine. Thus following the removal of the CBz groups using HBr in acetic acid, the use of this reagent increased the yield of guanidinylation from ~65% to over 70% of **7** at a much reduced cost of materials.

Finally, the reduction of the nitrile **7** to produce a primary amine for the attachment of diverse linkers was another low-yielding step from our previous route. The previous synthesis that used Raney nickel/H_2 resulted in 40–50% yields. Reduction using sodium borohydride catalyzed by cobalt chloride increased the yield of this step to ~60% of **8** (28,29). Amide coupling with the thiopyridylpropionic acid O-succinimide ester gave the desired thiopyridyl intermediate **9** and deprotection with TFA provided **10**. Synthesis of the disulfide **11** was easily accomplished in a two-step procedure with dithiothreitol (DTT) and then aerial oxidation.

The final optimized synthesis of 4G-SMoC is therefore shown in Figure 4. This improved method has enabled us for the first time to synthesize 4G-SMoC on a >200 mg scale.

Synthesis of simple SMoC analogs

The simple 1G- or 2G-SMoC derivatives were synthesized (Figure 5) using similar methods to those described earlier. Thus, simple alkylation utilizing the Cbz-protected mesylate **12** gave access to the simple monophenyl **13** and biphenyl **15–17** intermediates. Guanidylation and deprotection utilizing the aforementioned new reagent method gave **14** and **18–20**. These compounds were synthesized from commercially available mono- or biphenyl starting materials, eliminating the Suzuki coupling step.

6G-SMoC terphenyl analog synthesis

To maximize binding to siRNA, a new SMoC was synthesized with six guanidine groups attached to a triphenyl ring structure. The

6G-SMoC was synthesized (Figure 6) starting from the alkylated bromoiodocatechol synthesized previously (18) via coupling with the boronic ester, separation of the mono-22 and dicoupled product 21, and second coupling of the monocoupled product. This was followed by the deprotection of the Z-protecting groups and subsequent guanidinylation (30) to give **23**. Final removal of the Boc groups gave **24**.

Molecular dynamics

To gain more information about the structural conformation of the SMoC compounds, some simple SMoC-like structures were analyzed using the molecular dynamics software YASARA under the AMBER99 force field (Figure 7). It was found that in the case of a 2G-SMoC, possessing two guanidine side chains at the *ortho* position to the biphenyl bond, the guanidine groups form 'T-shaped' π-cation interactions with the opposite ring. This π-cation interaction is also seen in a 1G-SMoC structure with one guanidine side chain *ortho* to the biphenyl bond. However, when the side chain is moved to the *meta* position, the carbon chain is not long enough to allow interaction with the opposite ring, and a weaker 'parallel' π-cation interaction is seen between the guanidine and the adjacent ring. When only a single phenyl ring is present, no interaction occurs, suggesting that the electron density of one ring is insufficient to promote a π-cation interaction. These results suggest that the SMoC guanidinium ions may be stabilized by the presence of an additional phenyl ring (Figure 1), thus allowing stronger electrostatic interactions with siRNA. A movie of the molecular dynamics simulation is presented in the Supporting Information.

NMR pKa study

To investigate the strength of the proposed π-cation interaction, NMR was used to determine the pKa of SMoC guanidine groups by directly measuring the change in chemical shift of the adjacent methylene hydrogens (31,32). A change in the pKa of the guanidine would be expected if a π-cation interaction was present (31).

For each compound, the change in ionization state of the guanidine groups was measured using NMR by titrating each compound with sodium hydroxide and recording the ^{1}H chemical shifts of the CH_2 protons adjacent to the guanidine group against the pH of the solution (Figure 8). The pKa of the guanidine group is given by the Henderson–Hasselbalch equation (33):

$$\mathrm{pKa} = \mathrm{pH} + \log\frac{[\mathrm{BH}+]}{[\mathrm{B}]}$$

Deprotonation of the guanidine is expected to have a significant effect on the chemical shift of the protons on the adjacent methylene group because of the change in electron density around the nitrogen atom, resulting in increased shielding of the CH_2 protons. The chemical shift of the charged form (δB^+) may be determined by measuring the chemical shift at a low pH. For these compounds, the chemical shift was found to be at its maximum below pH 10. Likewise, at very high pH (pH 14), the chemical shift of the deprotonated guanidine groups may be measured (δB). Thus, the chemical shift at a given pH (δA) is representative of the proportion of groups that are protonated at a given time. Therefore, the equation may be expressed in terms of change in chemical shift:

$$\mathrm{pKa} = \mathrm{pH} + \log\frac{\delta\mathrm{A} - \delta\mathrm{B}}{\delta\mathrm{B}^+ - \delta\mathrm{A}}$$

Hence, by plotting the log of the ratio between the charged and uncharged forms expressed as chemical shifts against the pH of

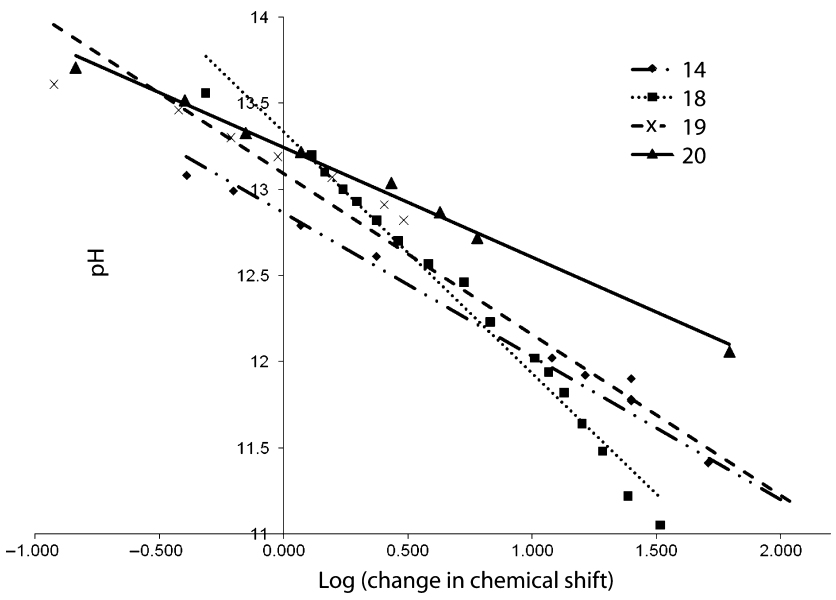

Figure 9: Hill plots to calculate small molecule carrier pKa values. The log of the ratio of uncharged to charged species expressed in terms of chemical shift plotted against the pH of the solution to find the pKa value as the *y*-intercept.

the solution (Figure 9), the pKa may be calculated from the *y*-intercept of the linear trend line.

The results of these experiments (Table 1) show that the 2G-SMoC with the biphenyl substituted at the ortho position to the biphenyl bond, **18**, has the highest pKa (13.33), suggesting that the guanidine groups in this compound benefit from the greatest stabilization. The monophenyl compound, **14** (12.86), has the lowest pKa and the closest to free arginine (12.48) (34), suggesting that very little stabilization is available to the guanidinium ion. These results also show that substitution position is also important for stabilization, because the meta-substituted compound, **19**, has a lower pKa (13.09) than the ortho-substituted compound **20** (13.26). These results suggest that the biphenyl system can provide some stabilization to the positively charged guanidinium ion. The energy of this stabilization may be calculated by comparing the pKa values of the monophenyl compound, **20**, and the mono-substituted biphenyl compound **19** using the equation:

$$\Delta\Delta G^0_{pKa} = 2.303RT\Delta pKa$$

This gives a free energy of stabilization of −2.3 kJ/mol for each guanidine group compared with the monophenyl compound, for which it was assumed that there is very little π-cation stabilization, owing to its low pKa. This value is the increase in the free energy of the guanidine group gained by the addition of a phenyl ring to the monophenyl compound **14**.

Table 1: pKa values calculated from the *y*-intercepts from Figure 3

Compound no.	Structure	pKa
14	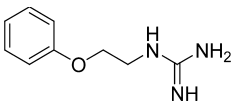	12.86
18	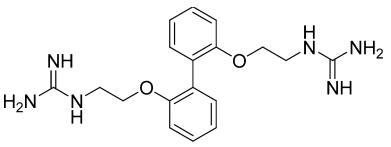	13.33
19	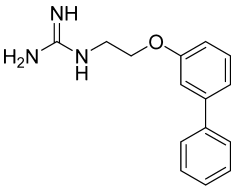	13.09
20	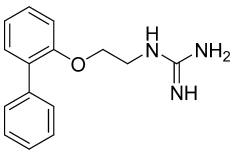	13.26

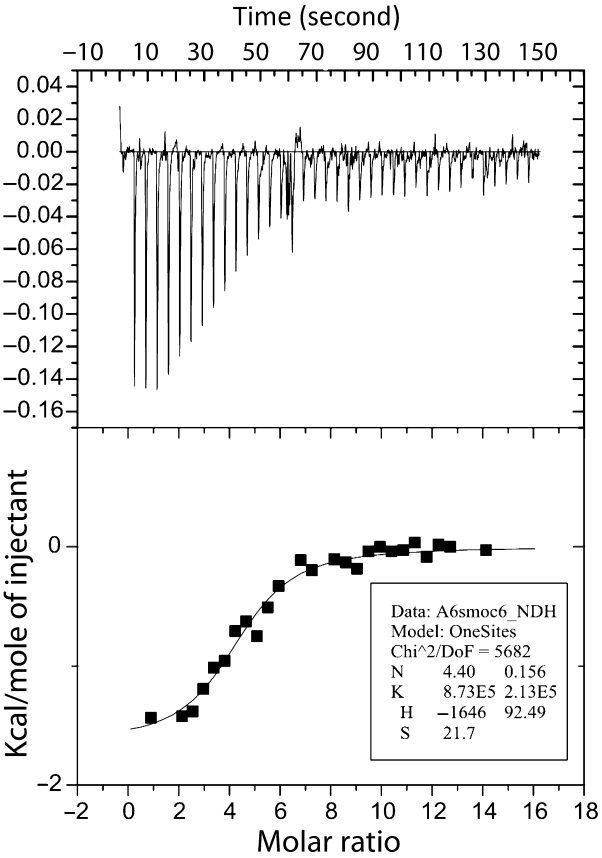

Figure 10: 6G-small molecule carrier (SMoC) isothermal calorimetry (ITC) binding curve. Above: ITC data for the titration of 6G-SMoC against human GAPD siRNA. Each spike represents the heat evolved upon a single 8-μL injection of 250 μM 6G-SMoC, **24**, into the calorimeter cell containing 3.5 μM GAPD siRNA. Below: The ORIGIN software was used to fit the ITC data to a binding curve and calculate the binding parameters.

ITC of 6G-SMoC indicates a high enthalpic contribution to binding

To calculate the strength of the interactions between SMoC and siRNA, ITC was used to measure the heat evolved when small aliquots of 6G-SMoC, **24**, were injected into a solution of a standard 21-bp siRNA (Figure 10). A binding constant (*K*) of 87.3 μM was calculated with a binding stoichiometry of 4.4:1 (SMoC/siRNA). Binding was dominated by enthalpic contributions (−1646 Kcal/mol) with a minor or negligible entropic contribution. This is consistent with electrostatic (charge) interactions between the guanidines and the phosphate groups on the siRNA dominating binding.

Gel shift studies on siRNA show that SMoCs can effectively complex with siRNA duplexes

The interactions of 4G- and 6G-SMoC compounds with siRNA were analyzed by gel electrophoresis of SMoC/siRNA complexes at different molar ratios. Tetra- and octa-arginine peptides were also tested to establish the relative binding affinity of SMoCs compared with these established cell delivery peptides. As shown in Figure 11, all

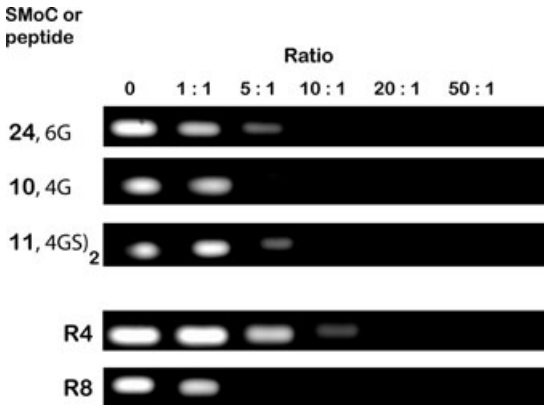

Figure 11: siRNA gel shift assay. Glyceraldehyde-3-phosphate dehydrogenase siRNA was mixed with small molecule carrier (SMoC) compounds or a polyarginine peptide (R4, R8) at the ratios shown with a running buffer containing ethidium bromide and run on a 1% agarose gel. The gels were visualized under UV illumination. SMoCs alone gave no signal (not shown).

SMoCs and peptides were able to fully shield the siRNA negative charges at ratios <20:1. As the observable band on the gel is proportional to the free siRNA concentration, we utilized this value to provide a convenient graphical representation of the relative affinities and to calculate the approximate binding constants of the analogs. The ethidium bromide (EtBr) fluorescence of each band was quantified, and the data were plotted as dose–response curves (Figure 12). 6G-SMoC, **24**, had a slightly lower binding affinity than 4G SMoC, **10**, (EC_{50} of 110 μM compared with 70 μM) and 4G-SMoC had a higher affinity than R4 (EC_{50} of 70 μM compared with 120 μM). However, R8 had a higher affinity (3 μM) than any of the SMoCs. The disulfide variant $(4G\text{-}SMoCS)_2$, **11**, has the same binding affinity as the monomer form, probably due to reduction of the disulfide bond in the gel running buffer. 4G-SMoC, **10**, binds with a higher affinity than the polyarginine peptide R4, indicating an ability to complex with siRNA more efficiently or to shield the negative charges more effectively. This may be attributed to the increased pKa of the SMoC guanidine groups as a result of the π-cation effect as described previously.

Confocal analysis of SMoC-mediated siRNA uptake

To determine whether siRNA/SMoC complexes are taken up by cells, the simple SMoCs described earlier were complexed with a fluorescently tagged siRNA oligo at concentrations of either 10 or 100 nM and incubated with IMR-90 cells, a diploid human fibroblast adherent cell strain derived from fetal lung tissue, for 24 h. Upon examination under confocal microscopy, only the 4G-SMoC compound **10** showed significant uptake (others not shown). For compound **10**, the fluorescent oligo was observed in the cytoplasm in a punctate distribution for both concentrations, showing that uptake occurs into vesicles, possibly endosomes formed via an endocytotic pathway (Figure 13).

siRNA/SMoC gene and protein knockdown

To determine whether SMoCs are capable of transporting siRNA into cells, IMR-90 cells were transfected with SMoC or Lipofectamine complexed with a double-stranded RNA oligo targeted at Cdc7, a cell cycle kinase that has been identified as a new cancer therapeutic target (35). Cancer cells establish only a limited number of DNA replication forks under Cdc7 rate-limiting conditions, causing fork stalling and collapse during an abortive S phase and triggering apoptotic cell death. Tumor cell specificity comes from normal cells avoiding lethal S-phase progression in the presence of low Cdc7 kinase levels by eliciting a p53-dependent replication origin activation checkpoint response that arrests the cells at the G1/S boundary (24). Seventy-two hours after the treatment, IMR90

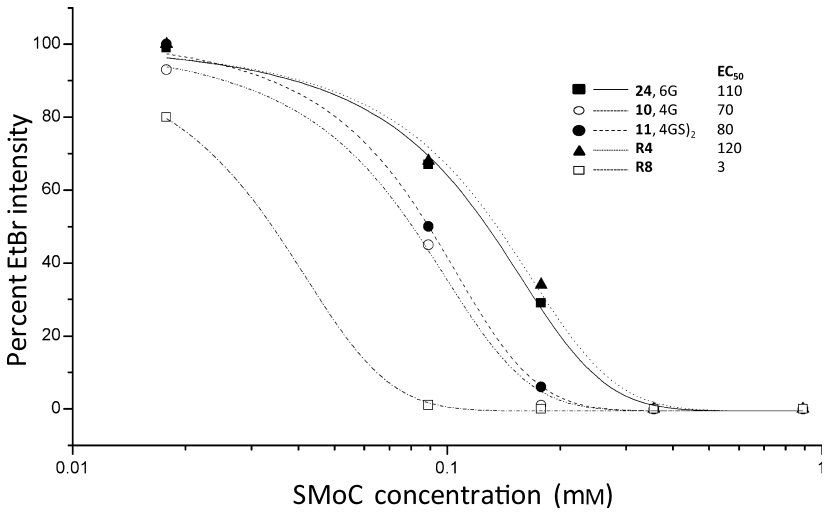

Figure 12: Binding curves derived from gel shift assay data. The EtBr bands were quantified, and the band intensity was plotted to produce binding curves for each of the compounds with siRNA. The EC_{50} and Hill coefficient (p) values of each compound are shown, giving a relative indication of the binding affinity of each compound to siRNA.

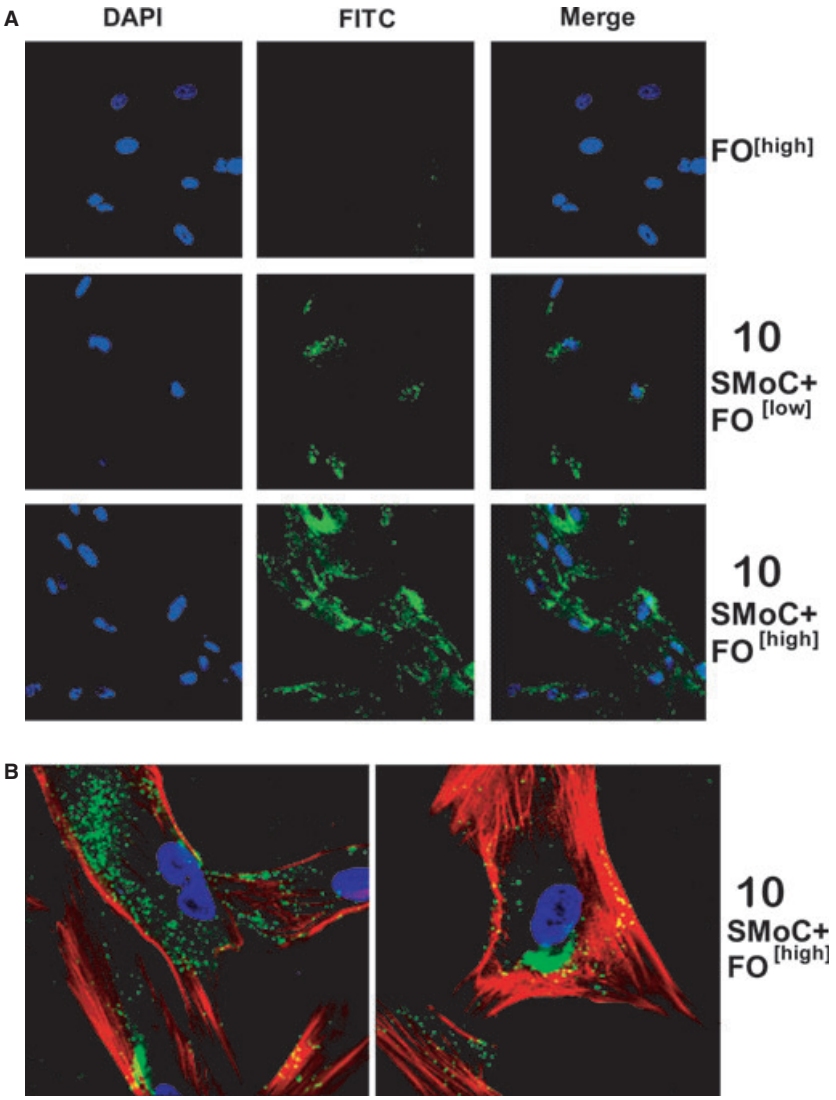

Figure 13: Intracellular delivery of fluorochrome-labeled siRNA (FO) by 4G-small molecule carrier (SMoC). (A) IMR-90 human diploid fibroblasts were cultured on coverslips and treated for 24 h with 100 nM FO ($FO^{[high]}$) or complexes of **10**, 4G-SMoC (40 μg/mL, 35 μM) and either 10 nM FO ($FO^{[low]}$) or 100 nM FO ($FO^{[high]}$). (B) IMR-90 cells treated with 100 nM FO ($FO^{[high]}$) in complex with **10**, SMoC and stained with DAPI and AlexaFluor 546 Phalloidin after fixation with paraformaldehyde.

cells were harvested, and CDC7 mRNA knockdown was monitored by qRT-PCR. For each compound tested, the CDC7 mRNA level was determined relative to control cells treated only with Lipofectamine or SMoC. Different concentrations of 4G-SMoC **10** were tested in conjunction with 10 nM CDC7-siRNA, and a final concentration of 35 μM was found to result in a CDC7 knockdown efficiency of 61% comparable with that achieved with Lipofectamine 2000 (80% knockdown as determined by qRT-PCR). These results were similar to the CDC7 knockdown achieved with Lipofectamine plus CDC7-siRNA, which reduced mRNA levels by 80% (Figure 14A). The transfection experiments utilized 40 μg/mL of SMoC (35 μM) with 10–100 nM of siRNA. A ratio of at least 350:1. The ratio of charges is 42 (negative charges on the siRNA phosphates) to 4 (guanidine groups on the SMoC) or ~10:1 Thus, the ratio of charges is 35 (positive) to 1 and the complexes are positively charged.

RNAi against CDC7, mediated through 4G-SMoC or Lipofectamine, caused an accumulation of IMR90 cells with G1 DNA content and a concomitant reduction in the S-phase fraction, while the fraction of cells with <2C DNA content was negligible, indicating that the Cdc7-depleted cells remained viable (Figure 14B). We recently demonstrated the triggering of an origin activation checkpoint in Cdc7-depleted IMR90 cells (24). Consistent with this study, Western blotting of extracts prepared from IMR90 cells treated with complexes of 4G-SMoC, **10**, and CDC7-siRNA showed that phosphorylation of the replication initiation factor Mcm2 at the Cdc7-dependent phosphor-site Ser-40/41 was markedly reduced when Cdc7 kinase and its regulatory subunit ASK were downregulated. In keeping with the activation of the origin activation checkpoint in the Cdc7-depleted cells, we also noted p53 stabilization and increased levels of the cyclin dependent kinase (CDK) inhibitor protein p21 (Fig-

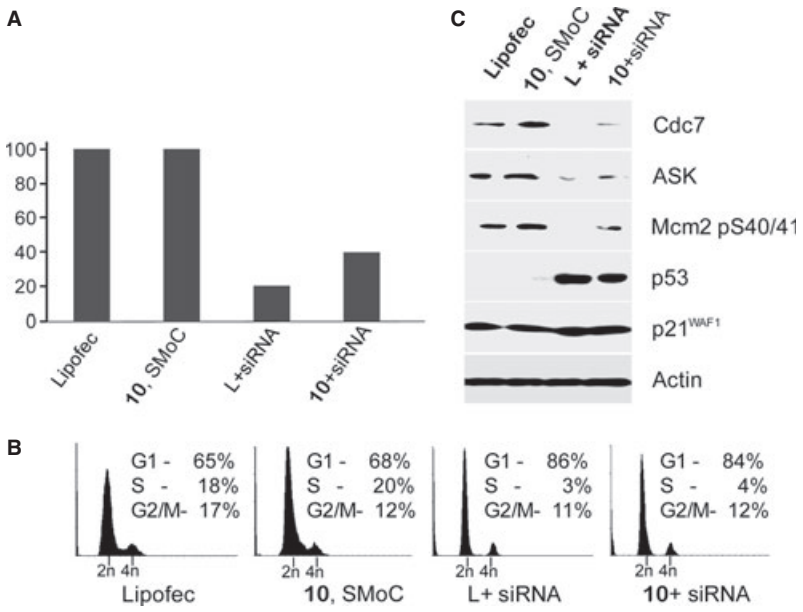

Figure 14: CDC7 knockdown phenotype in IMR90 cells after small molecule carrier (SMoC)-mediated uptake of CDC7-siRNA. (A) IMR-90 fibroblasts were treated for 72 h with complexes of either Lipofectamine 2000 or 4G-SMoC **10**, with CDC7-siRNA. Lipofectamine 2000 and **10** alone were used as controls. Knockdown of CDC7 transcript levels was confirmed by qRT-PCR relative to Lipofectamine only and **10**, only treatment. (B) DNA content of Lipofectamine-treated cells (Lipofec), **10**-treated cells, and cells treated with complexes of Lipofectamine and CDC7-siRNA (L + siRNA) or **10** and CDC7-siRNA (**10** + siRNA). (C) Whole-cell extracts prepared from Lipofec, **10**-treated, L + siRNA, and **10** + siRNA cells were analyzed by immunoblotting with the indicated antibodies (β-actin – loading control).

ure 14C). Taken together, these data demonstrate that SMoCs are capable of mediating the uptake of siRNAs into cultured human cells without altering their biological activity. Note that 6G-SMoC, **24**, was also tested for siRNA transfection but did not result in significant knockdown (data not shown).

Conclusions

The SMoC class of compounds, modeled on amphipathic CPPs, have previously been shown to transport active proteins as well as conjugated dyes into a variety of cell types (18). Here, we have improved the synthetic route to the SMoC compounds, including the use of Molander chemistry in the form of a stable trifluoroborate intermediate that can be used to easily build new, varied SMoC-like structures, as well as the optimization of some of the previously difficult steps to increase the scale of the synthesis.

We have also shown in this study that SMoCs show potential as siRNA transfection agents. One surprise from this study is that the most effective delivery and knockdown were achieved with the 4G-SMoC, compound **10** where the thiopyridyl group is commonly regarded as a reactive protein thiol reagent. An improvement in CPP delivery has been noted for some cysteine-containing peptides (36) where dimerization or oligimerization is indicated. In addition, enhancement of internalization has been noted for CPPs containing cysteines conjugated with the 2-nitropyridyl group (37). An interaction with cell-surface thiols was suggested for this observation, and we speculate that compound **10** may also interact with cell-surface thiols to promote internalization.

siRNA delivery remains a significant challenge in biological therapeutics, and an effective transfection agent will open up a vast array of possibilities in the treatment for many diseases by specifically targeting the underlying genetic malfunctions. The standard *in vitro* transfection agent Lipofectamine is demonstrably toxic, by several measures (38) indicating the need for further research in this area. Cell-penetrating peptides show a great deal of promise as transfection agents, and many studies have successfully introduced siRNA into cells using both covalently and non-covalently linked CPPs (8). As CPP mimics, it is therefore likely that SMoCs will also possess this ability to act as siRNA delivery vectors, possessing positively charged guanidine groups that allow the formation of electrostatic complexes with siRNA and are also essential for successful passage across the cell membrane. Our MD and NMR studies indicate that the guanidinium ions on the SMoC side chains are stabilized by π-cation. The potential impact of π-cation effects has also been advanced for the Arg–Trp interaction in the penetratin CPP (39). We probed the affinity of the SMoC–siRNA interaction using two methods ITC (the gold standard for evaluating binding interactions) and simple gel shift analysis. These were in good agreement indicating binding affinities in the range 70–110 μM. The polyarginine peptide R8 had an affinity of 30 μM. The optimal binding affinity for SMoC/siRNA delivery remains to be determined. As we show here, SMoCs can deliver biologically active siRNA into cultured human cells and achieved RNAi knockdown with a similar

magnitude to the widely used Lipofectamine reagent. Further optimization of SMoCs to increase the uptake of SMoC/siRNA complexes will be reported in due course.

Acknowledgments

We thank the Association for International Cancer Research (AICR) for funding this project (Grant Ref: 06-0076). This work was also partly funded by Cancer Research UK Scientific Programme Grant C428/A6263 (KS and GHW). We would also like to thank Tina Divita and Matt Webster of the ISMB Biophysics Centre at Birkbeck College for their assistance with the ITC work.

References

1. Guo J., Fisher K.A., Darcy R., Cryan J.F., O'Driscoll C. (2010) Therapeutic targeting in the silent era: advances in non-viral siRNA delivery. Mol Biosyst;6:1143–1161.
2. Whitehead K., Langer R., Anderson D. (2009) Knocking down barriers: advances in siRNA delivery. Nat Rev Drug Discov;8:129–138.
3. Sontheimer E.J. (2005) Assembly and function of RNA silencing complexes. Nat Rev Mol Cell Biol;6:127–138.
4. Li W., Szoka F.C. (2007) Lipid-based nanoparticles for nucleic acid delivery. Pharm Res;24:438–449.
5. Rozema D.B., Lewis D.L., Wakefield D.H., Wong S.C., Klein J.J., Roesch P.L., Bertin S.L., Rappen T.W., Chu Q., Blokhin A.V., Hagstrom J.E., Wolff J.A. (2007) Dynamic polyconjugates for targeted in vivo delivery of siRNA to hepatocytes. Proc Natl Acad Sci USA;104:12982–12987.
6. Kim S.W., Kim N.Y., Choi Y.B., Park S.H., Yang J.M., Shin S. (2010) RNA interference in vitro and in vivo using an arginine peptide/siRNA complex system. J Control Release;143:335–343.
7. Konate K., Crombez L., Deshayes S., Decaffmeyer M., Thomas A., Brasseur R., Aldrian G., Heitz F., Divita G. (2010) Insight into the cellular uptake mechanism of a secondary amphipathic cell-penetrating peptide for siRNA delivery. Biochemistry;49:3393–3402.
8. Eguchi A., Dowdy S.F. (2009) siRNA delivery using peptide transduction domains. Trends Pharmacol Sci;30:341–345.
9. Veldhoen S., Laufer S.D., Trampe A., Restle T. (2006) Cellular delivery of small interfering RNA by a non-covalently attached cell-penetrating peptide: quantitative analysis of uptake and biological effect. Nucleic Acids Res;34:6561–6573.
10. Crombez L., Aldrian-Herrada G., Konate K., Nguyen Q.N., McMaster G.K., Brasseur R., Heitz F., Divita G. (2009) A new potent secondary amphipathic cell-penetrating peptide for siRNA delivery into mammalian cells. Mol Ther;17:95–103.
11. Gump J.M., June R.K., Dowdy S.F. (2010) Revised role of glycosaminoglycans in TAT protein transduction domain-mediated cellular transduction. J Biol Chem;285:1500–1507.
12. Jiao C.Y., Delaroche D., Burlina F., Alves I.D., Chassaing G., Sagan S. (2009) Translocation and Endocytosis for Cell-penetrating Peptide Internalization. J Biol Chem;284:33957–33965.
13. El-Sayed A., Khalil I.A., Kogure K., Futaki S., Harashima H. (2008) Octaarginine- and octalysine-modified nanoparticles have different modes of endosomal escape. J Biol Chem;283:23450–23461.
14. Chao T.-Y., Raines R.T. (2011) Mechanism of ribonuclease a endocytosis: analogies to cell-penetrating peptides. Biochemistry;50:8374–8382.
15. Duchardt F., Fotin-Mleczek M., Schwarz H., Fischer R., Brock R. (2007) A comprehensive model for the cellular uptake of cationic cell-penetrating peptides. Traffic;8:848–866.
16. Burley S.K., Petsko G.A. (1986) Amino-aromatic interactions in proteins. FEBS Lett;203:139–143.
17. Gallivan J.P., Dougherty D.A. (1999) Cation-pi interactions in structural biology. Proc Natl Acad Sci USA;96:9459–9464.
18. Rebstock A.S., Visintin C., Leo E., Posada C.G., Kingsbury S.R., Williams G.H., Stoeber K., Selwood D.L. (2008) Modular assembly using sequential palladium coupling gives easy access to the SMoC class of cellular transporters. ChemBioChem;9: 1787–1796.
19. Okuyama M., Laman H., Kingsbury S.R., Visintin C., Leo E., Eward K.L., Stoeber K., Boshoff C., Williams G.H., Selwood D.L. (2007) Small-molecule mimics of an [alpha]-helix for efficient transport of proteins into cells. Nat Methods;4:153–159.
20. Lundberg P., El Andaloussi S., Sutlu T., Johansson H., Langel U. (2007) Delivery of short interfering RNA using endosomolytic cell-penetrating peptides. FASEB J;21:2664–2671.
21. Krieger E., Koraimann G., Vriend G. (2002) Increasing the precision of comparative models with YASARA NOVA – a self-parameterizing force field. Proteins;47:393–402.
22. Wang J.M., Cieplak P., Kollman P.A. (2000) How well does a restrained electrostatic potential (RESP) model perform in calculating conformational energies of organic and biological molecules? J Comput Chem;21:1049–1074.
23. Kingsbury S.R., Loddo M., Fanshawe T., Obermann E.C., Prevost A.T., Stoeber K., Williams G.H. (2005) Repression of DNA replication licensing in quiescence is independent of geminin and may define the cell cycle state of progenitor cells. Exp Cell Res;309:56–67.
24. Tudzarova S., Trotter M.W.B., Wollenschlaeger A., Mulvey C., Godovac-Zimmermann J., Williams G.H., Stoeber K. (2010) Molecular architecture of the DNA replication origin activation checkpoint. EMBO J;29:3381–3394.
25. Wang X.J., Sun X.F., Zhang L., Xu Y.B., Krishnamurthy D., Senanayake C.H. (2006) Noncryogenic I/Br-Mg exchange of aromatic halides bearing sensitive functional groups using i-PrMgCl-bis 2-(*N,N*-dimethylamino)ethyl ether complexes. Org Lett;8:305–307.
26. Molander G.A., Figueroa R. (2005) Organotrifluoroborates: expanding organoboron chemistry. Aldrichimica Acta;38:49–56.
27. Molander G.A., Ellis N. (2007) Organotrifluoroborates: protected boronic acids that expand the versatility of the Suzuki coupling reaction. Acc Chem Res;40:275–286.
28. Ducatel H., Van Nhien A.N., Postel D. (2008) Novel glycine like amino acids from glyco-[alpha]-aminonitriles as building blocks for peptide synthesis. Tetrahedron: Asymmetry;19:67–81.
29. Feldman K.S., Ngernmeesri P. (2005) Dragmacidin E synthesis studies. Preparation of a model cycloheptannelated indole fragment. Org Lett;7:5449–5452.
30. Feichtinger K., Sings H.L., Baker T.J., Matthews K., Goodman M. (1998) Triurethane-protected guanidines and triflyldiurethane-protected guanidines: new reagents for guanidinylation reactions. J Org Chem;63:8432–8439.

31. Acharya P., Plashkevych O., Morita C., Yamada S., Chattopadhyaya J. (2003) A repertoire of pyridinium-phenyl-methyl cross-talk through a cascade of intramolecular electrostatic interactions. J Org Chem;68:1529–1538.
32. Oganesyan A., Cruz I.A., Amador R.B., Sorto N.A., Lozano J., Godinez C.E. *et al.* (2007) High yield selective acylation of polyamines: proton as protecting group. Org Lett;9:4967–4970.
33. Atkins P., de Paula J. (2002) Atkins' Physical Chemistry, 7th edn. Oxford: Oxford University Press.
34. Kumaki Y., Nitta K., Hikichi K., Matsumoto T., Matsushima N. (2004) Side chain-side chain interactions of arginine with tyrosine and aspartic acid in Arg/Gly/Tyr-rich domains within plant glycine-rich RNA binding proteins. J Biochem;136:29–37.
35. Swords R., Mahalingam D., O'Dwyer M., Santocanale C., Kelly K., Carew J. *et al.* (2010) Cdc7 kinase – a new target for drug development. Eur J Cancer;46:33–40.
36. Won Y.-W., Kim H.A., Lee M., Kim Y.-H. (2010) Reducible Poly(oligo-D-arginine) for enhanced gene expression in mouse lung by intratracheal injection. Mol Ther;18:734–742.
37. Aubry S., Aussedat B., Delaroche D., Jiao C.Y., Bolbach G., Lavielle S. *et al.* (2010) MALDI-TOF mass spectrometry: a powerful tool to study the internalization of cell-penetrating peptides. Biochim Biophys Acta-Biomembr;1798:2182–2189.
38. Eguchi A., Meade B.R., Chang Y.C., Fredrickson C.T., Willert K., Puri N. *et al.* (2009) Efficient siRNA delivery into primary cells by a peptide transduction domain-dsRNA binding domain fusion protein. Nat Biotechnol;27:567–U110.
39. Lensink M.F., Christiaens B., Vandekerckhove J., Prochiantz A., Rosseneu M. (2005) Penetratin-membrane association: W48/R52/W56 shield the peptide from the aqueous phase. Biophys J;88:939–952.

Supporting Information

Additional Supporting Information may be found in the online version of this article:

Appendix S1. Full experimental details of chemistry syntheses.

Movie S1. Molecular dynamics simulation of a 2G-SMoC molecule showing the effect of a pi-cation interaction on conformation.

Please note: Wiley-Blackwell is not responsible for the content or functionality of any supporting materials supplied by the authors. Any queries (other than missing material) should be directed to the corresponding author for the article.